land

MDPI

Article

Quantifying the Drivers of Vegetation Resilience Gradient Effects Across Hierarchical Administrative Borders: A Case Study of the Beijing–Tianjin–Hebei Region

Lifu Zheng †, Yunlu Zhang *,†, Ruojing Li, Kaiping Wang, Siqi Wu, Tieyue Qiang and Luxuan Lei

School of Landscape Architecture, Beijing Forestry University, Beijing 100083, China; zhenglifu@bjfu.edu.cn (L.Z.); lrj0123@bjfu.edu.cn (R.L.); wangkaiping@bjfu.edu.cn (K.W.); wsq547@bjfu.com (S.W.); 15175753274@163.com (T.Q.); leiluxuan@bjfu.edu.cn (L.L.)

* Correspondence: zhangyunlu@bjfu.edu.cn

† These authors contributed equally to this work.

Abstract

Understanding vegetation resilience gradient effects across hierarchical administrative borders is critical for cross-jurisdictional land management yet remains underexplored. This study integrates an AR(1) model with XGBoost-SHAP analysis to assess resilience and its drivers across provincial, municipal, and county borders in the Beijing–Tianjin–Hebei (BTH) region using NDVI data (2000–2025). The results show that (1) vegetation resilience across hierarchical border belts experienced an initial decline followed by recovery. A notable shift in resilience optimality was observed from city borders in 2005 to provincial borders by 2020. Gradient effects were stronger in northern city borders. The stable-fluctuating type dominated, followed by peak and valley types. (2) Precipitation, tree age, and altitude suppress gradient formation. Conversely, cross-boundary economic disparity, nighttime light differences, and land use composition tend to be associated with amplified gradient effects in a hierarchical manner: cropland and built-up expansion intensify gradients at provincial borders but reduce them at city borders, suggesting a potential role of governance coordination. (3) Based on these findings, a tiered governance framework is suggested—northern high-gradient provincial and city borders are proposed as priority areas for intensive interventions, while county borders (where gradient effects are weakest) may benefit from moderate, low-intensity interventions focused on maintaining land use continuity. At the provincial level, stronger inter-provincial coordination—through cross-boundary ecological compensation and harmonized environmental standards—may help mitigate gradient effects. Collectively, this study provides insights for cross-jurisdictional land governance in the BTH region and other analogous urban agglomerations.

Keywords: vegetation resilience; administrative border belts; ecological gradients; spatial heterogeneity; Beijing–Tianjin–Hebei region

Check for updates

Academic Editor: Shiliang Liu

Received: 18 May 2026
Revised: 24 June 2026
Accepted: 27 June 2026
Published: 22 July 2026

Copyright: © 2026 by the authors. Licensee MDPI, Basel, Switzerland. This article is an open access article distributed under the terms and conditions of the Creative Commons Attribution (CC BY) license.

1. Introduction

Vegetation resilience is a key metric for evaluating ecological restoration outcomes and sustaining regional ecosystem stability [1–3]. While substantial research has focused on vegetation resilience dynamics within watersheds or urban systems, the spatial behavior of resilience within administrative border zones remains largely unexplored [4]. This knowledge gap is concerning, as such border areas are not peripheral but functionally significant. Take the Beijing–Tianjin–Hebei (BTH) region as an example. Based on the calculation using

2020 gridded GDP and population data, a 30 km wide buffer along provincial boundaries houses approximately 28.82 million people and contributes about 22.00% of the region's GDP, forming a distinct "border socio-ecological system". Yet, fragmented governance due to overlapping administrative mandates hinders accurate resilience assessment and effective cross-boundary coordination [5]. This institutional gap directly undermines progress toward SDGs 15 and 17, which call for sustainable ecosystem management and transboundary partnership [6,7]. Addressing this gap requires a systematic understanding of vegetation resilience dynamics within these governance transition zones—a scientific challenge essential for advancing integrated cross-jurisdictional environmental management.

Recently, vegetation resilience in administrative border areas has garnered increasing scholarly attention [8,9]. Previous studies have provided a foundational basis for evaluating vegetation resilience performance, primarily emphasizing overall recovery status and temporal evolution patterns [10–12]. Nevertheless, the spatial heterogeneity of vegetation resilience across administrative borders—particularly concerning gradient typologies, magnitude variations, and spatial extent—remains inadequately characterized. More importantly, it remains unclear whether gradient effects differ significantly across administrative levels (provincial–provincial, city–city, and county–county borders), and which level exhibits the most pronounced boundary influence.

A deeper gap concerns the mechanisms driving these gradient configurations, particularly the interplay between environmental and socioeconomic factors in shaping gradient intensity [13]. While it is widely accepted that vegetation resilience in border regions results from long-term biophysical and human interactions [14,15], the specific pathways through which terrain complexity, climate variability, economic growth, and land-use pattern jointly influence gradient structures remain poorly understood [16–18].

This study focuses on three hierarchical administrative border belts in the BTH region: provincial–provincial, city–city, and county–county boundaries. Considering their spatial scales, buffer zones extending 15 km, 10 km, and 5 km on each side were established, respectively. Based on annual NDVI datasets from 2000 to 2025 and the first-order autoregressive [AR(1)] model, vegetation resilience was estimated for 2005, 2010, 2015, and 2020. Gradient patterns were modeled using GAM, with gradient types classified and intensity quantified. A combined XGBoost-SHAP framework integrated with Random Forest modeling was applied to evaluate the contributions of natural and socioeconomic factors to gradient type and intensity across the three administrative levels. This study addresses three objectives: (1) characterizing the spatiotemporal distribution of vegetation resilience across the three border belts; (2) identifying systematic gradient patterns, determining spatial range thresholds, and conducting comparative analyses across administrative levels; and (3) examining how drivers interact to shape gradient type and intensity across hierarchical borders. The findings are anticipated to establish a scientific foundation for strengthening cross-jurisdictional ecological governance and supporting differentiated management strategies across administrative levels.

2. Materials and Methods

2.1. Study Area

The study area, covering approximately 187,432 km^2, comprises buffer belts extending 15 km, 10 km, and 5 km on each side of provincial, city, and county administrative boundaries within the BTH region, respectively (Figure 1). The hierarchical buffer zones were delineated using ArcGIS 10.6 and subsequent data processing and statistical modeling were implemented in Python 3.10. The selection of hierarchical buffer widths follows the spatial scales of different administrative levels and avoids the incorporation of urban built-up areas in county-level analysis. The study area exhibits pronounced spatial heterogeneity in

land use patterns across its border belts. In the southern belts (Hebei–Shandong–Henan), cropland dominates with interspersed urban and rural built-up areas, where agricultural activities and urbanization exert strong influences on vegetation resilience. In the western belts (Hebei–Shanxi), located in the Taihang Mountains, forest ecosystems prevail with high vegetation cover but complex terrain, where ecological restoration and forest management are primary determinants of resilience. In the northwestern belts (Hebei–Inner Mongolia), situated in an agro-pastoral ecotone, grassland and desertified land dominate under fragile ecological conditions, where vegetation resilience is highly sensitive to climate variability and grazing intensity. In the belts surrounding Beijing (Hebei–Beijing), forest ecosystems dominate due to capital function decentralization and ecological barrier construction, with extensive distribution of ecological public welfare forests and water conservation forests under substantial ecological restoration investment. These diverse natural and land use contexts provide an ideal natural laboratory for systematically comparing vegetation resilience gradient effects across hierarchical administrative border belts.

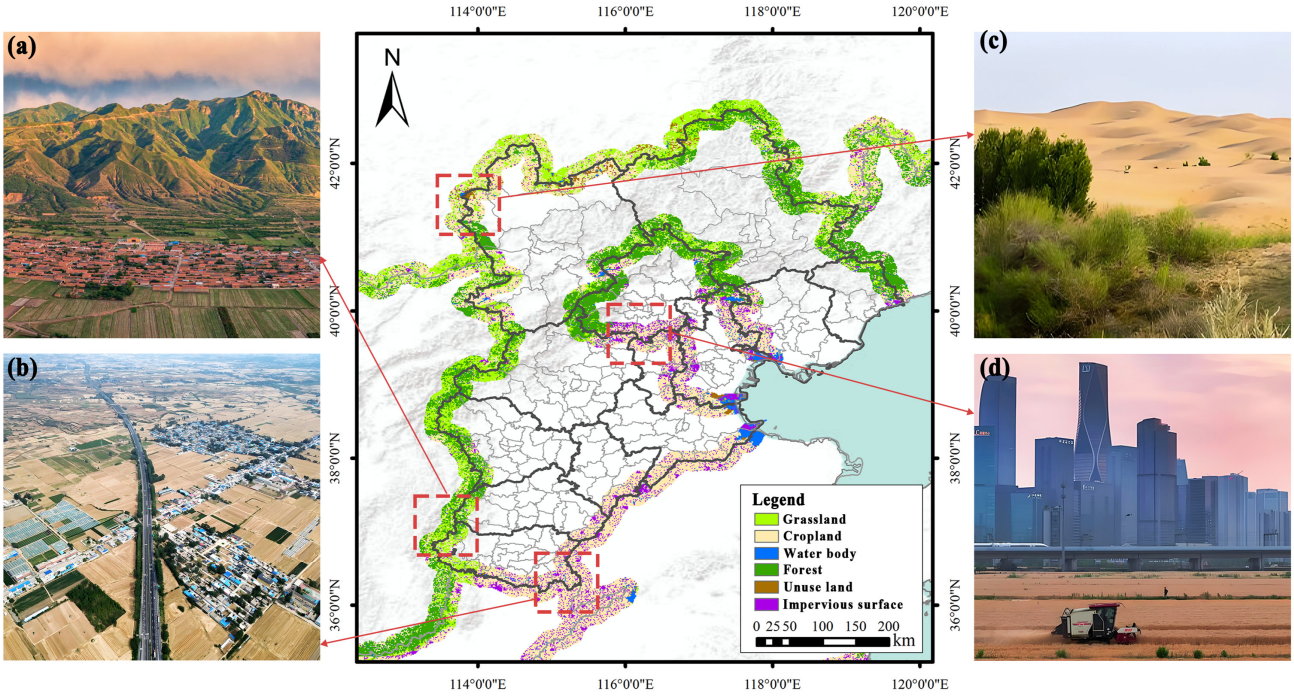


Figure 1. Study area. (**a**) Interprovincial border belts between Shanxi and Hebei; (**b**) interprovincial border belts among Hebei, Shandong, and Henan; (**c**) interprovincial border belts between Inner Mongolia and Hebei; (**d**) interprovincial border belts between Beijing and Hebei.

2.2. Data Sources

This study employs multiple datasets, including administrative boundary vectors, annual NDVI data [19], and various socioeconomic and environmental indicators (Table 1). Socioeconomic datasets consist of population density, GDP, nighttime light intensity, and road network vectors. Environmental datasets include annual precipitation, annual temperature, digital elevation model (DEM), soil organic matter, soil moisture, soil clay content, tree age, and biodiversity integrity index. Based on these datasets, 21 candidate explanatory variables were derived and grouped into socioeconomic and natural environmental categories. To ensure spatial consistency and comparability across all variables, each indicator was standardized and resampled to a uniform spatial resolution of 1 km. A summary of all potential influencing factors and their corresponding data sources is provided in the table below.

Table 1. Data sources and potential influencing factors.

	Category	Data Sources	Original Spatial Resolution	Data Source References
Socioeconomic indicators	Total GDP (TG)	GDP data per year	1 km	[20]
	Total nighttime (TN) lighting	Data on nighttime lighting per year	1 km	[21]
	Average road network (AR)	Road network data	-	[22]
	Proportion of land designated for construction (PC)	Land-use data	30 m	
	Lateral total GDP difference (LG)	GDP data per year	1 km	-
	Lateral total night-time lighting difference (LN)	Data on nighttime lighting per year	1 km	-
	Lateral average road network (LR) difference	Road network data	-	-
	Economic radiation intensity (EI)	GDP data per year	1 km	Mean interpolated GDP within the border belt
	Cross-boundary economic disparity (ED)	GDP data per year	1 km	Absolute GDP difference between the two sides of the border
Natural environmental indicators	Five-year mean precipitation (MP)	Annual precipitation data	1 km	[23]
	Five-year mean temperature (MT)	Annual temperature data	1 km	[24]
	Average tree age (TA)	Tree age dataset	1 km	[25]
	Lateral mean biodiversity integrity index difference (LB)	Biodiversity integrity index dataset	1 km	-
	Lateral mean altitude difference (LA)	DEM data	30 m	-
	Mean biodiversity integrity index (MB)	Biodiversity integrity index dataset	1 km	[26]
	Mean altitude (MA)	DEM data	30 m	[27]
	Proportion of farmland (PF)	Land-use data	30 m	-
	Proportion of grassland (PG)	Land-use data	30 m	-
	Mean soil organic matter content (SOM)	Dataset of soil properties for land surface modeling over China	5 km	[28]
	Mean soil clay content (CC)		5 km	
	Mean soil moisture content (SM)		5 km	

2.3. Methods

To determine the appropriate buffer widths for each administrative level, we tested alternative distances of 5, 10, 15, and 20 km on both sides of the boundaries. The selected widths (15 km for provincial, 10 km for city, and 5 km for county borders) were identified as optimal for capturing peak and valley gradient patterns, as narrower buffers failed to capture full gradient transitions while wider buffers introduced noise from non-boundary-related ecological variation (Figure S2). A total of 3264 border belt samples were delineated at regular intervals across the study area. Vegetation resilience was quantified using the first-order autoregressive [AR(1)] model, which is grounded in temporal autocorrelation theory. Subsequently, Generalized Additive Models (GAM) were employed to fit the spatial variation curves of vegetation resilience across the border belts. Five gradient types and their corresponding intensities were identified based on predefined classification rules. The spatial range thresholds of gradient effects were determined using Pettitt change-point detection. Finally, a combined XGBoost-SHAP framework integrated with Random Forest modeling was applied to analyze the influence mechanisms of socioeconomic and natural environmental factors on gradient types and intensities across the three administrative levels (Figure 2).

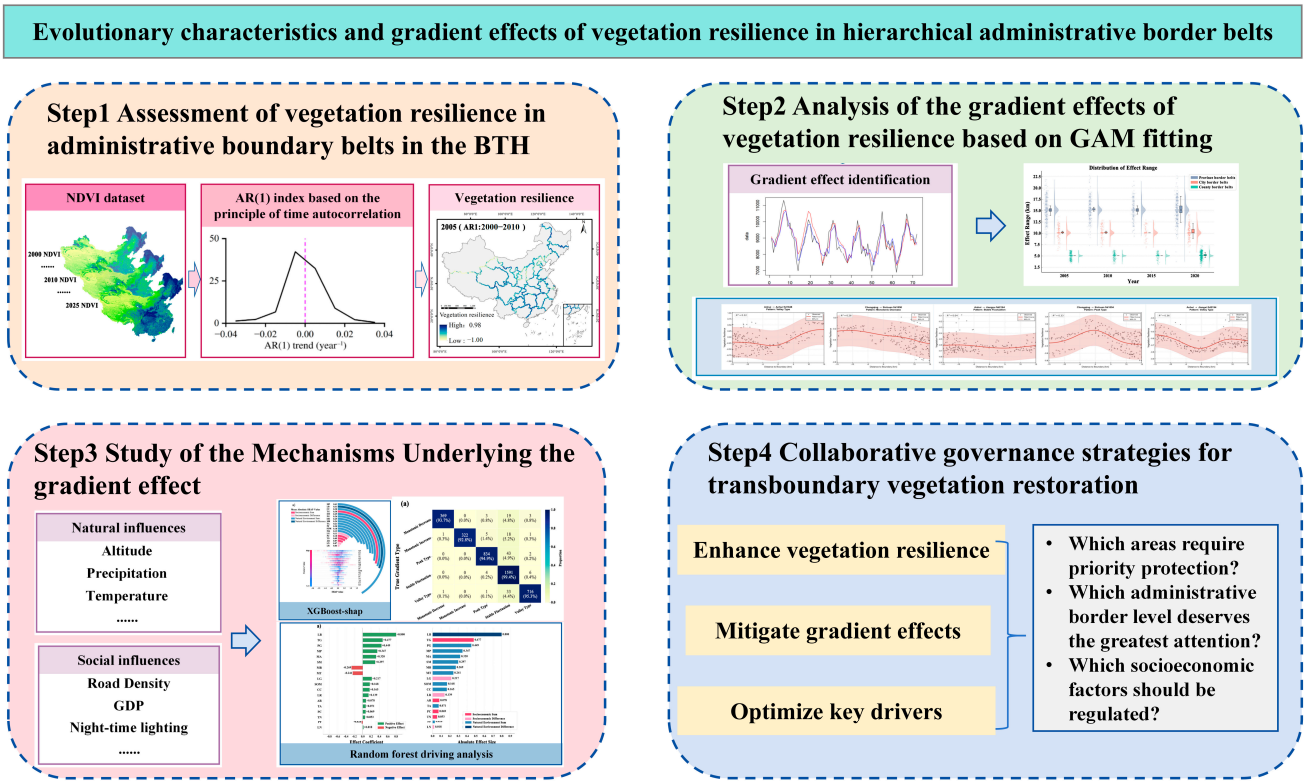


Figure 2. The conceptual framework of the study.

2.3.1. Vegetation Resilience Assessment

Vegetation resilience is critical for recovering ecosystem structure and function after disturbance. In this study, resilience is quantified using an autocorrelation-based approach, centered on a first-order autoregressive (AR(1)) model of NDVI time series with a moving 10-year window for each target year (2000–2010 for 2005; 2005–2015 for 2010; 2010–2020 for 2015 and 2020) [29]. While adjacent windows partially overlap, this design provides sufficient temporal coverage to estimate ecosystem recovery dynamics while smoothing interannual climatic variability. The calculation is grounded in the "memory effect" theory of ecosystems: if an ecosystem exhibits high resilience, its current state depends less on past

states, corresponding to weak autocorrelation; conversely, strong autocorrelation indicates lower resilience. The resilience index is defined as:

$$\text{Resilience} = -r \quad (1)$$

where ρ is the first-order autocorrelation coefficient of the NDVI time series, obtained via linear regression:

$$\text{NDVI}_t = \propto + \beta \times \text{NDVI}_{t-1} + \in_t \quad (2)$$

Here, NDVI_t and NDVI_{t-1} represent the normalized difference vegetation index of the current year and the previous year, respectively. $\propto$ represents the baseline contribution of environmental conditions to NDVI, β is the autoregressive coefficient reflecting the temporal persistence of vegetation state, and $\in_t$ denotes the random error term capturing environmental fluctuations and disturbance events not explained by historical states.

2.3.2. Quantification of Vegetation Resilience Gradient Types and Effect Intensity in Hierarchical Border Belts

To capture and identify the nonlinear relationship between vegetation resilience and distance from administrative boundaries at different hierarchical levels (provincial, city, and county), this study employed Generalized Additive Models (GAM) for curve fitting and pattern recognition [30,31]. GAM allows flexible nonlinear associations between response and predictor variables, with the general form expressed as:

$$y_i = \beta_0 + f(x_i) + \in_i \quad (3)$$

where y_i is the observed vegetation resilience, x_i denotes the perpendicular distance of the sampling point to the administrative boundary, $f(\cdot)$ represents smooth functions describing nonlinear effects and $\in_i$ is the random error term.

Based on the fitted GAM curves, five gradient types were classified according to geometric and statistical criteria, including overall slope, location of extrema, and deviation from linearity. Monotonic decreasing: curve exhibits a significant overall decline (normalized slope < -0.5) without notable upward fluctuations. Monotonic increasing: curve shows a significant overall rise (normalized slope > 0.5) without notable downward fluctuations. Peak type: curve displays a pronounced convex peak within 5 km from the boundary (maximum positive deviation > 0.25). Valley type: curve exhibits a distinct concave dip within 5 km from the boundary (maximum negative deviation < -0.25). Stable fluctuating: curve remains relatively flat (range < 0.12) or shows no significant directional trend.

To compare the effect intensity across different gradient types, type-specific metrics were applied. Monotonic types were characterized by the mean absolute gradient, reflecting the rate of change. Peak and valley types were quantified by the range (maximum − minimum) to capture fluctuation amplitude. The stable fluctuating type was measured by the standard deviation, indicating the degree of variability. All intensity values were normalized to a 0–1 scale for comparability.

To further quantify the spatial extent of gradient effects, the spatial range threshold—defined as the distance from the boundary at which vegetation resilience fluctuations stabilize—was determined using Pettitt change-point detection. This nonparametric test identifies statistically significant breakpoints in the fitted GAM curves separately for the left (negative distance) and right (positive distance) sides. The total effect range was calculated as the sum of absolute left and right thresholds, representing the full width of the boundary influence zone. The threshold was considered significant only when $p < 0.05$.

2.3.3. Mechanisms of Gradient Effect and Intensity

Subsequently, the study applied an interpretable machine learning classifier (XGBoost-SHAP) to analyze the influence of socioeconomic and natural environmental factors on the formation of the five gradient types within each administrative level [32]. In the classifier, the stable fluctuating type was assigned as class 1, while the four gradient types—monotonic increasing, monotonic decreasing, peak, and valley—were collectively treated as class 2, jointly representing the manifestation of gradient effects. The model was configured with 150 estimators, a maximum depth of 6, and a learning rate of 0.1, and optimized using a binary logistic loss function:

$$L(y, \hat{y}) = \sum_{i=1}^{n} \left[y_i \log(\hat{y}_i) + (1 - y_i) \log(1 - \hat{y}_i) \right] \quad (4)$$

where y_i denotes the true binary label and $\hat{y}_i$ represents the predicted probability of gradient type formation. The model was trained separately within each climatic zone to capture region-specific ecological dynamics, and its performance was evaluated through accuracy metrics and confusion matrices. For each observation and feature, the SHAP value quantifies the marginal contribution of that feature to the prediction relative to the average prediction:

$$\varnothing_{ij} = \sum_{S \subseteq N \setminus \{j\}} \frac{|S|!(|N| - |S| - 1)!}{|N|!} [f(S \cup \{j\}) - f(S)] \quad (5)$$

where N is the set of all features, S denotes a subset of features, and $f(S)$ represents the model prediction using only the features in subset S. The mean absolute SHAP value was computed to quantify feature importance:

$$\text{importance}_i = \frac{1}{n} \sum_{i=1}^{n} |\varnothing_{ij}| \quad (6)$$

Finally, the study used a random forest model to examine the mechanisms influencing gradient-effect intensity [33,34]. Initially, the 21 driving factors were aggregated into four latent variables: Socioeconomic Sum, Socioeconomic Difference, Natural Sum, and Natural Difference. A random forest regression model was then built to capture the nonlinear relationship between gradient-effect intensity and each driver:

$$\hat{y} = f_{RF}(x_1, x_2, \ldots, x_p) \quad (7)$$

where f_{RF} represents an ensemble of 200 decision trees, each constructed by recursively partitioning the data to minimize mean squared error. The number of trees was selected based on monitoring out-of-bag error stabilization, and the model performance was evaluated using R^2 and RMSE on the test set. To quantify the influence of each factor on gradient-effect intensity, a standardized influence coefficient was derived by combining feature importance from the random forest model with the directional information provided by Pearson correlation coefficients. Specifically, the influence coefficient for factor j was calculated as:

$$c_j = \frac{\text{Imp}_j}{\sum_k \text{Imp}_k} \cdot \text{sgn}(r_j) \quad (8)$$

where Imp_j denotes the Gini importance of factor j from the random forest model, and $\text{sgn}(r_j)$ is the sign of the Pearson correlation coefficient between factor j and the target variable, indicating whether the factor exerts a positive or negative effect. The resulting coefficients were normalized to a range of approximately $[-0.5, 0.5]$ to facilitate cross-factor comparison. Additionally, the 21 factors were aggregated into four latent variable

groups—Socioeconomic Sum, Socioeconomic Difference, Natural Sum, and Natural Difference—to evaluate the composite effects of each category on gradient-intensity formation.

3. Results

3.1. Spatiotemporal Patterns of Vegetation Resilience

Figure 3 illustrates the spatial distribution and temporal dynamics of vegetation resilience across the three hierarchical administrative border belts (provincial, city, and county) in the BTH region from 2005 to 2020. Overall, vegetation resilience displayed substantial spatial heterogeneity and a declining pattern over the study period, with a recovery observed in 2020.

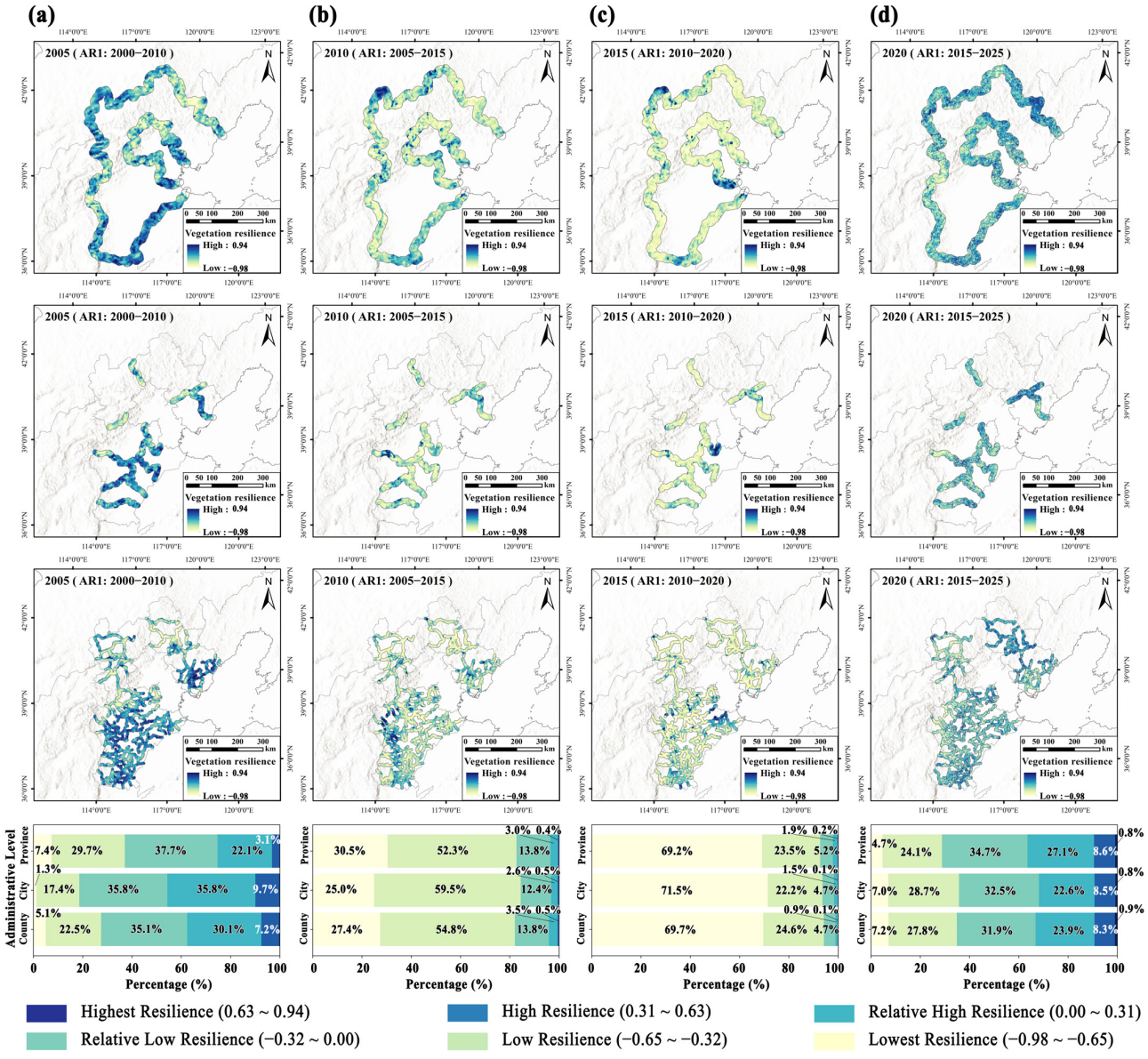


Figure 3. Spatiotemporal dynamics of vegetation resilience within the BTH region: (**a**) 2005; (**b**) 2010; (**c**) 2015; (**d**) 2020.

In 2005, high-resilience belts in provincial border zones produced relatively contiguous clusters, primarily located along the southeastern Hebei–Shandong border. In 2010 and 2015, the high-resilience areas shifted to the northwestern Inner Mongolia–Hebei border. By 2020, high-value zones became concentrated in the northeastern tri-junction area of Inner Mongolia–Hebei–Liaoning. For city border belts, high-resilience areas in 2005 were predominantly concentrated in the southern parts, notably along borders such as Shijiazhuang–Baoding and Hengshui–Cangzhou. Between 2010 and 2015, vegetation resilience significantly declined across city borders, whereas by 2020, high-resilience zones re-emerged in the northeast, particularly along the Chengde–Tangshan and Chengde–Qinhuangdao borders. For county border belts, the highest vegetation resilience in 2005 was observed in the southern and northeastern county borders. During 2010–2015, high-resilience areas were mainly concentrated along county borders adjacent to Shanxi Province, and by 2020, they had shifted to the northeastern county borders within Chengde City.

From a proportional perspective, notable differences emerged across the three administrative levels. In 2005, city border belts exhibited the highest vegetation resilience status overall, with the combined proportion of relatively high resilience and above reaching 45.5%. In contrast, provincial and county border belts accounted for only 25.2% and 37.3%, respectively. Between 2010 and 2015, the proportion of relatively high resilience areas declined across all three hierarchical border belts. By 2020, provincial border belts had become the most resilient, with the combined share of relatively high resilience and above reaching 36.5%, followed by county border belts at 33.1% and city border belts at 31.8%.

3.2. Gradient Effects of Vegetation Resilience

Figures 4 and 5 show the composition, spatial configuration, and magnitude of gradient types across the three hierarchical administrative border belts (provincial, city, and county) in the BTH region for 2005, 2010, 2015, and 2020. The effective range of gradient effects was 15.12 km for provincial borders, 10.07 km for city borders, and 5.03 km for county borders (Figure S1). Across all three levels, the stable-fluctuating type was consistently predominant, followed by the peak and valley types, whereas monotonic increasing and decreasing types remained comparatively rare throughout the study period. Provincial border belts exhibited significantly stronger gradient effects than city and county belts in 2005, with the combined proportion of peak and valley types exceeding 50.65%, compared to only 44.08% and 25.92% for city and county belts, respectively. Subsequently, in 2010 and 2015, gradient effects declined markedly across all three hierarchical levels. In 2010, the stable-fluctuating type accounted for over 51.83% of city and county belts and 41.81% of provincial belts. By 2015, the stable-fluctuating type had further increased to over 67.74% in city and county belts and 57.59% in provincial belts, with provincial borders still exhibiting stronger gradient effects than city and county borders. By 2020, city border belts displayed slightly stronger gradient effects than provincial and county belts, with the combined proportion of peak and valley types reaching 47.10%, monotonic types accounting for 22.15%, and stable-fluctuating type comprising 30.75%. Meanwhile, provincial border belts exhibited 46.23% for peak and valley types, 18.49% for monotonic types, and 35.28% for stable-fluctuating types.

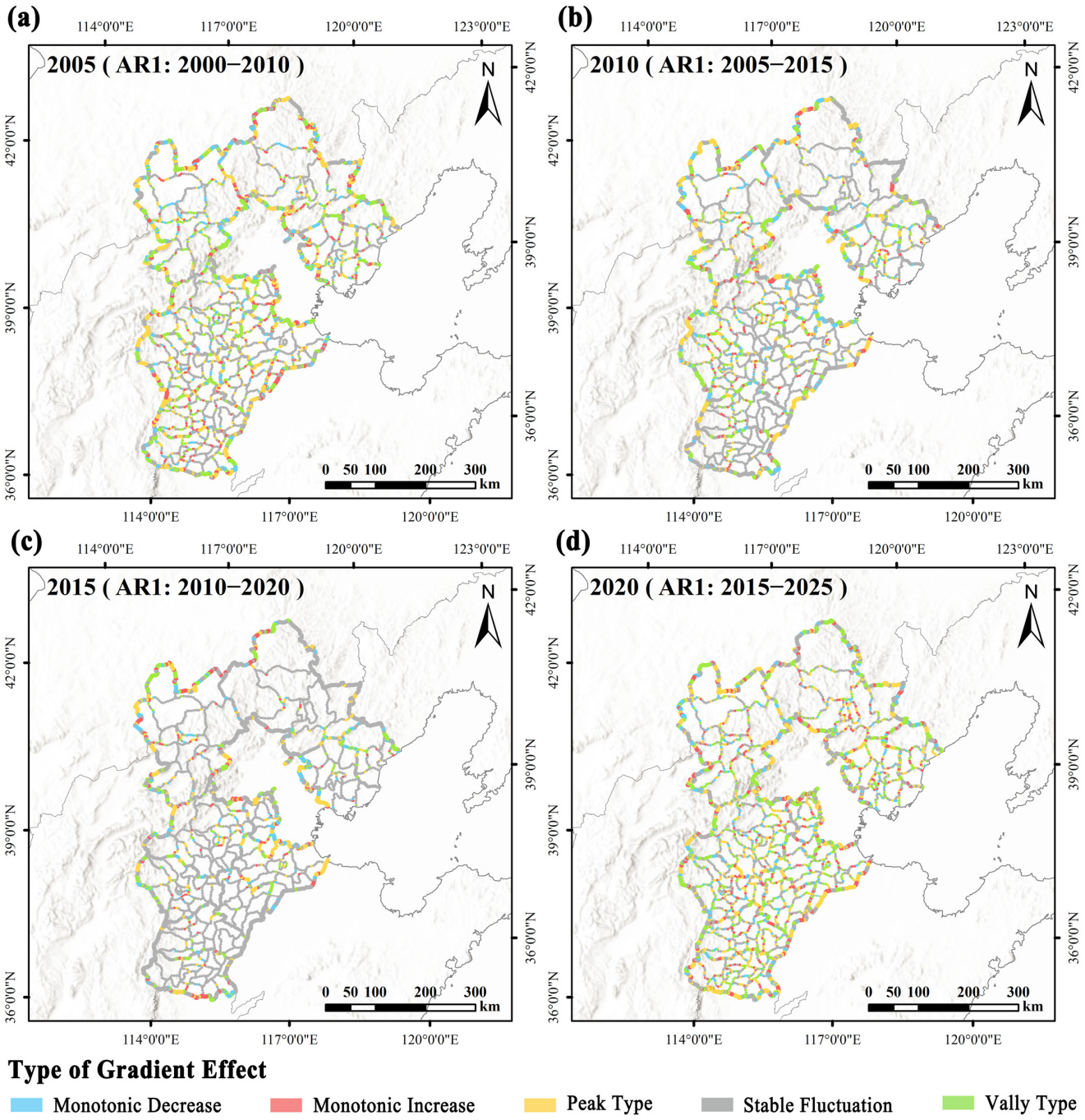


Figure 4. Spatial distribution of vegetation resilience gradient types within the BTH region across four periods: (**a**) 2005; (**b**) 2010; (**c**) 2015; (**d**) 2020.

Figure 6 presents the average proportion of gradient effect types within cities. The results reveal that vegetation resilience gradient effects were generally stronger in the northern part of the BTH region than in the southern part. Specifically, cities such as Zhangjiakou, Tangshan, Langfang, and Qinhuangdao exhibited consistently stronger gradient effects across the study period. The proportion of unstable fluctuating types in Zhangjiakou averaged 45.80% across 2005–2020, ranking among the highest of all cities. Tangshan followed closely with an average of 43.53%, with notably high proportions in 2005, 2010, and 2020. Langfang and Qinhuangdao also showed elevated levels, with averages of 43.20% and 40.68%, respectively. In the southern part, Shijiazhuang and Baoding showed relatively strong effects, with Xingtai, Handan, and Hengshui displaying the weakest gradient effects.

By 2020, the gradient effects in city and county border belts had increased substantially, surpassing the levels observed in 2005.

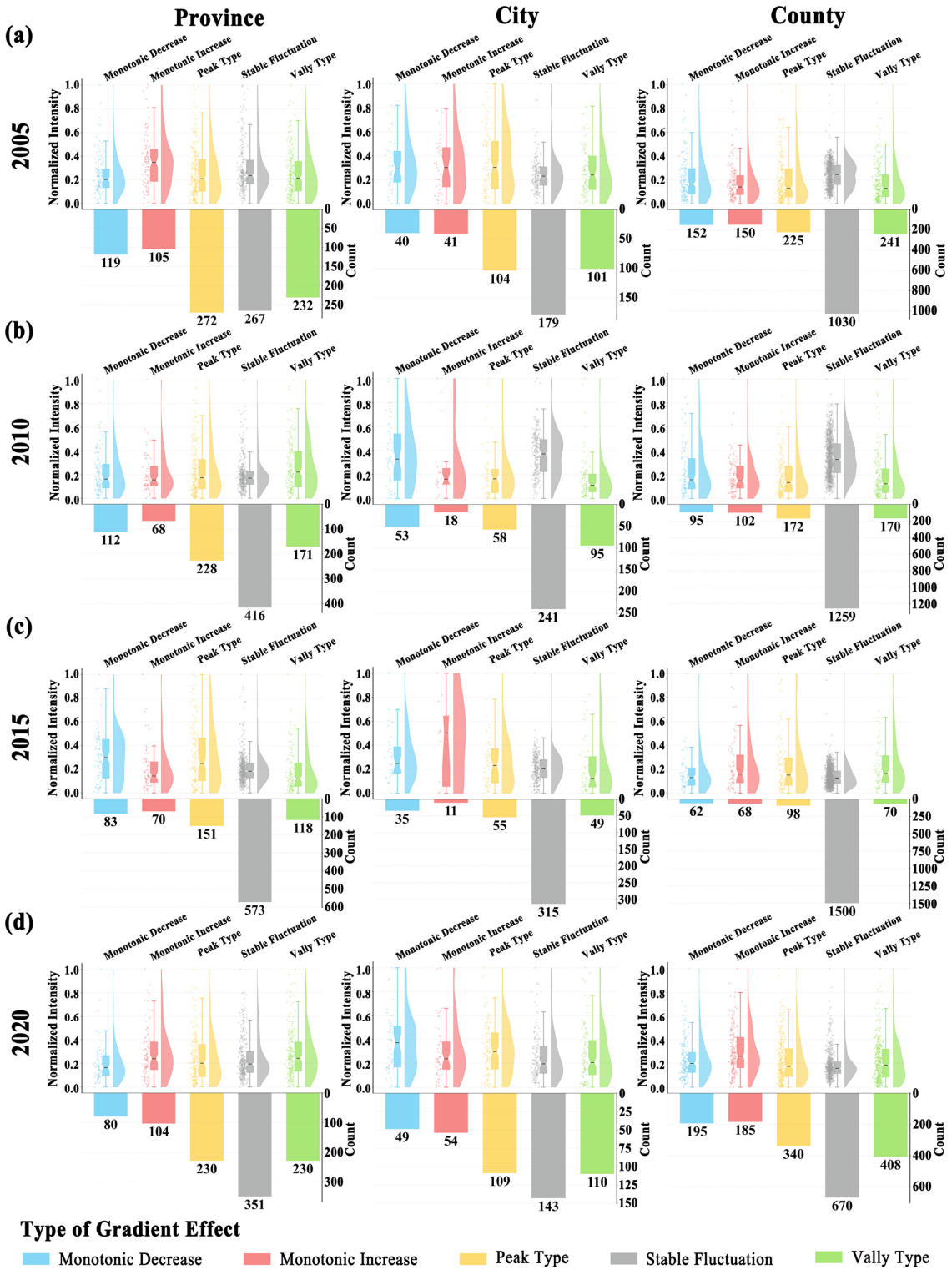


Figure 5. Effect magnitudes and frequency distributions of vegetation resilience gradient types at multiple administrative levels (provincial, city, and county): (**a**) 2005; (**b**) 2010; (**c**) 2015; (**d**) 2020.

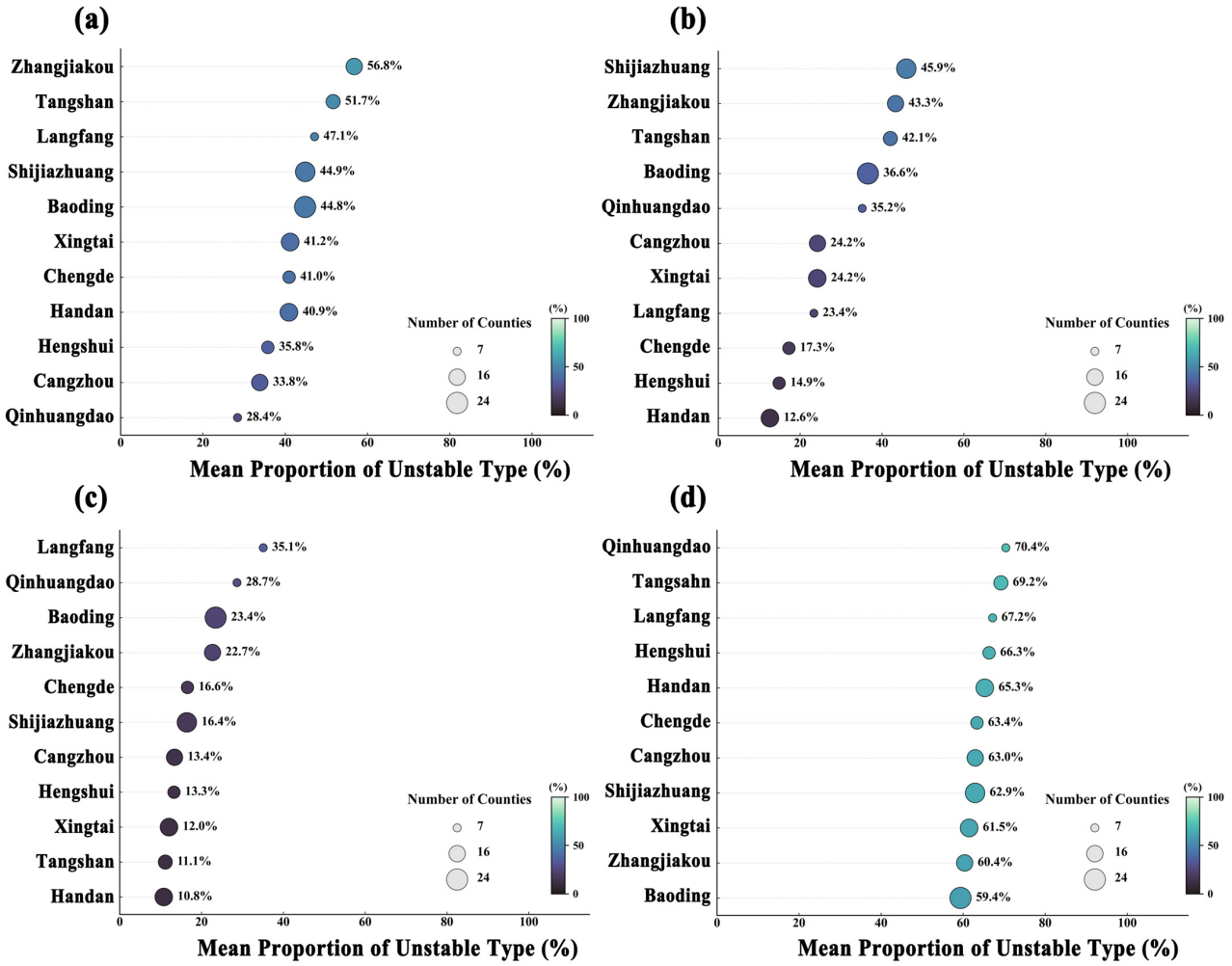


Figure 6. Statistics on the proportion of vegetation resilience gradient types showing unstable fluctuation gradients across cities within the BTH region: (**a**) 2005; (**b**) 2010; (**c**) 2015; (**d**) 2020.

From 2005 to 2020, vegetation resilience and gradient effects exhibited an inverse relationship across administrative levels. In 2005, city border belts showed higher resilience but weaker gradient effects (peak and valley types at 44.08%), whereas provincial belts displayed lower resilience yet stronger gradient effects (peak and valley types exceeding 50.65%). By 2020, this pattern had reversed: provincial belts had become more resilient with weaker gradient effects (46.23%), while city belts showed stronger gradient effects (47.10%) despite lower resilience.

To assess the robustness of our classification framework, we conducted a sensitivity analysis by systematically varying the three key thresholds across all four study periods from 2005 to 2020 (Figure 7). The results demonstrate that the classification is highly stable with respect to slope and deviation threshold variations, with sample reclassification rates remaining below 6% for slope and below 1.3% for deviation across most years. Although the range threshold exhibited relatively higher sensitivity with 14.5% to 37.5% of samples reclassified, this is expected given its direct role in distinguishing the dominant stable-fluctuating type, which consistently comprised 37.3% to 83.4% of samples across years. More importantly, the temporal patterns remained consistent regardless of threshold selection. The stable-fluctuating type dominated in 2005, 2010, and 2015 with proportions of 70.0%, 70.0%, and 83.4%, respectively, followed by a marked decline to 37.3% in 2020. This decline was accompanied by substantial increases in monotonic types from approximately 5% to 10% each and peak and valley types from approximately 9% to 19% and 9% to

23%, respectively. These consistent temporal trajectories across diverse threshold settings confirm that our classification results are robust and reflect genuine ecological changes rather than artifacts of arbitrary parameter selection.

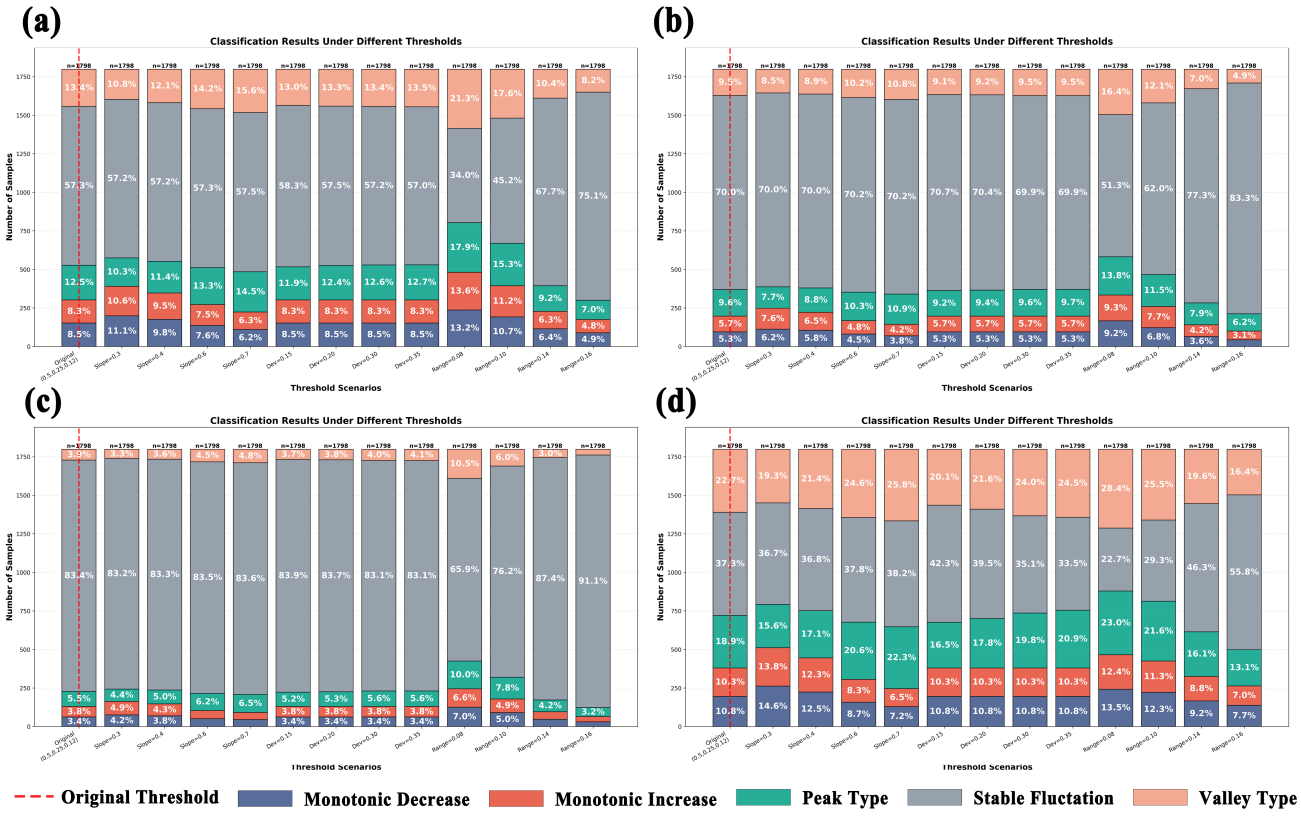


Figure 7. Sensitivity analysis of county-level gradient type classification results for (**a**) 2005, (**b**) 2010, (**c**) 2015, and (**d**) 2020.

The land use composition within the border belts corresponding to each gradient category was further examined (Figure 8). Overall, the land use composition across the three hierarchical border belts was dominated by cropland, forest, grassland, and built-up surfaces. From 2005 to 2020, city and county belts consistently exhibited higher proportions of cropland and built-up area than provincial belts. Specifically, built-up area accounted for an average of 12.09% and 15.78% in city and county belts, respectively, compared to 8.16% in provincial belts; cropland occupied 59.52% and 52.76% versus 43.38%. In contrast, forest and grassland were more prevalent in provincial belts, with forest coverage averaging 23.32%, substantially exceeding the 15.44% and 14.85% observed in city and county belts. Over the study period, forest proportion increased slightly in provincial belts but declined modestly in city and county belts, while cropland in city and county belts showed an initial decrease followed by a subsequent recovery. Built-up area expanded across all three administrative levels.

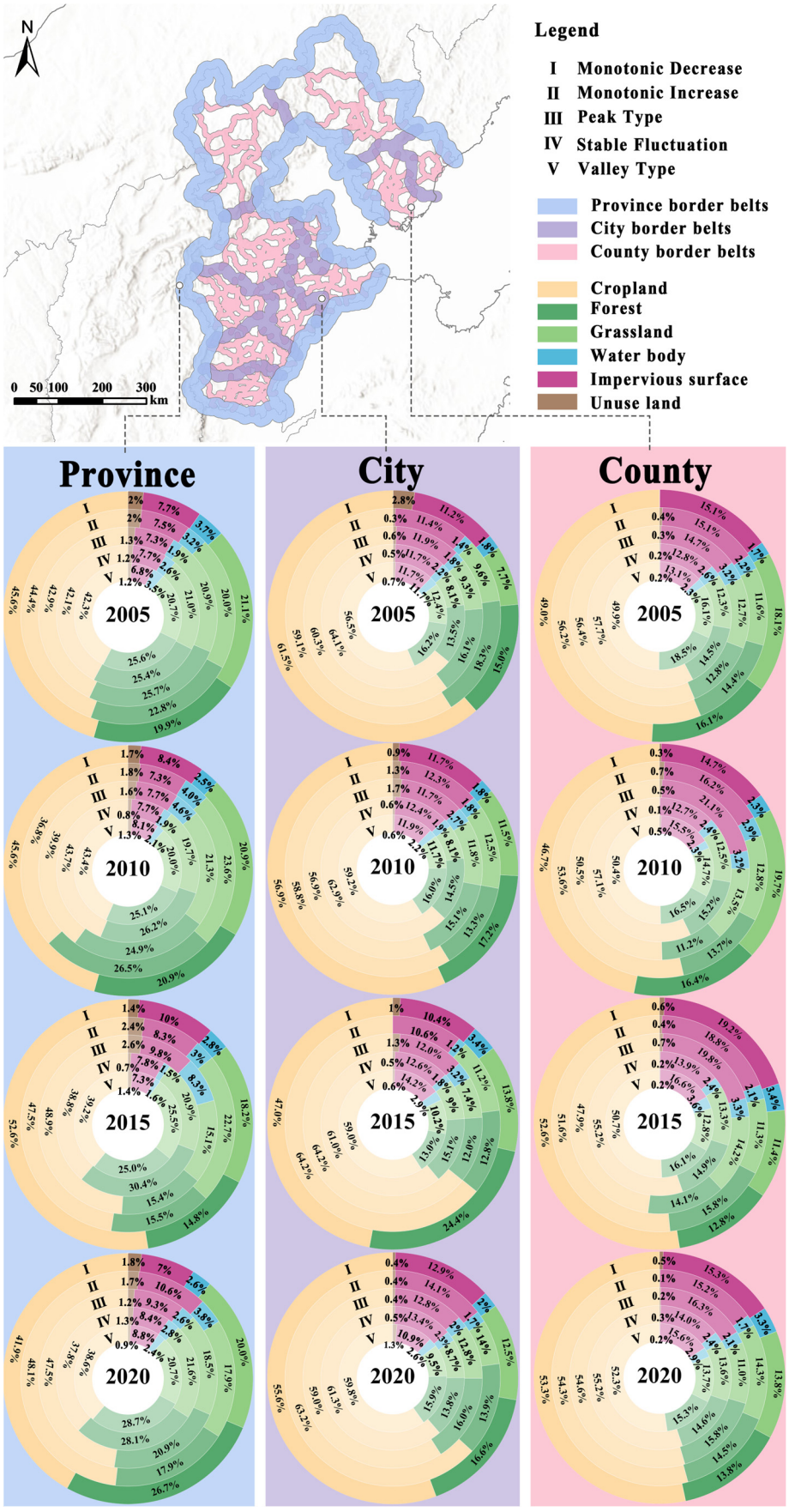


Figure 8. Land use composition of different gradient types across hierarchical administrative borders in the BTH region.

Based on the gradient type comparison, the stable-fluctuating type exhibited the lowest proportion of unused land (0.57%), compared to monotonic increase (1.1%), monotonic decrease (0.97%), peak type (1.03%), and valley type (0.74%). The monotonic increase, monotonic decrease, and valley types showed the highest forest and grassland coverage, at 17.49%, 16.46%, and 16.80%, respectively, exceeding those of the peak type (15.35%) and stable-fluctuating type (15.87%). In contrast, the peak type had the highest impervious surface proportion (12.86%), higher than monotonic increase (11.98%), monotonic decrease (12.32%), valley type (11.71%), and stable-fluctuating type (11.25%). These patterns imply that an increase in unused land may amplify gradient effects along administrative boundaries. In border zones with higher forest and grassland coverage, vegetation resilience is more likely to reflect cross-boundary disparities in management intensity or governance effectiveness, giving rise to monotonic increase, monotonic decrease, or valley type gradient patterns. Conversely, the expansion of built-up surfaces near the boundary often signals improved vegetation management and maintenance conditions, which tends to foster peak type gradient patterns of vegetation resilience.

3.3. Gradient Effects and Intensity Attribution

Based on Moran's I spatial autocorrelation analysis, we assessed the potential influence of spatial dependence among the 21 explanatory variables and the target variable of gradient types. The results showed that only 4 out of 21 factors exhibited significant spatial autocorrelation with $p < 0.05$, including mean soil moisture content SM, mean soil clay content CC, average road network AR, and lateral total night-time lighting difference LN, with Moran's I values of 2.7599, 0.9670, 1.2091, and −0.4725, respectively. The remaining 17 factors showed no significant spatial clustering. More importantly, the target variable of gradient types exhibited no significant spatial autocorrelation with Moran's I = 0.0202 and $p = 0.3990$, indicating that the classification of gradient types is not spatially clustered.

The XGBoost classifier achieved overall accuracies of 0.965, 1.000, and 0.900 for provincial, city, and county borders, respectively (Figure S3), indicating reliable model performance for SHAP-based driver interpretation across all administrative levels. The results reveal interpretable patterns in the drivers of vegetation resilience gradient formation across the BTH region, with model performance falling within the range commonly reported in ecological gradient studies (Figure 9). For provincial border belts, mean annual precipitation (MP, 0.27) and average tree age (TA, 0.14) exert significant suppressive effects on gradient effects, whereas cross-boundary economic disparity (ED, 0.16) and the difference in nighttime light intensity (LN, 0.13) are associated with intensified gradient formation. For city border belts, in addition to the suppressing effects of MP (0.37) and TG (0.21), higher soil moisture (SM, 0.18) and cropland proportion (PF, 0.17) also mitigate gradient effects. Conversely, mean temperature (MT, 0.19) and cross-boundary biodiversity disparity (LB, 0.16) play promoting roles in gradient development. For county border belts, MP (0.34) remains the dominant factor in eliminating gradient effects, with mean biodiversity integrity (MB, 0.15) also exerting a moderating influence. Meanwhile, increased nighttime light intensity (TN, 0.17) and a larger cross-boundary economic disparity (ED, 0.13) tend to amplify gradient effects along county-level borders.

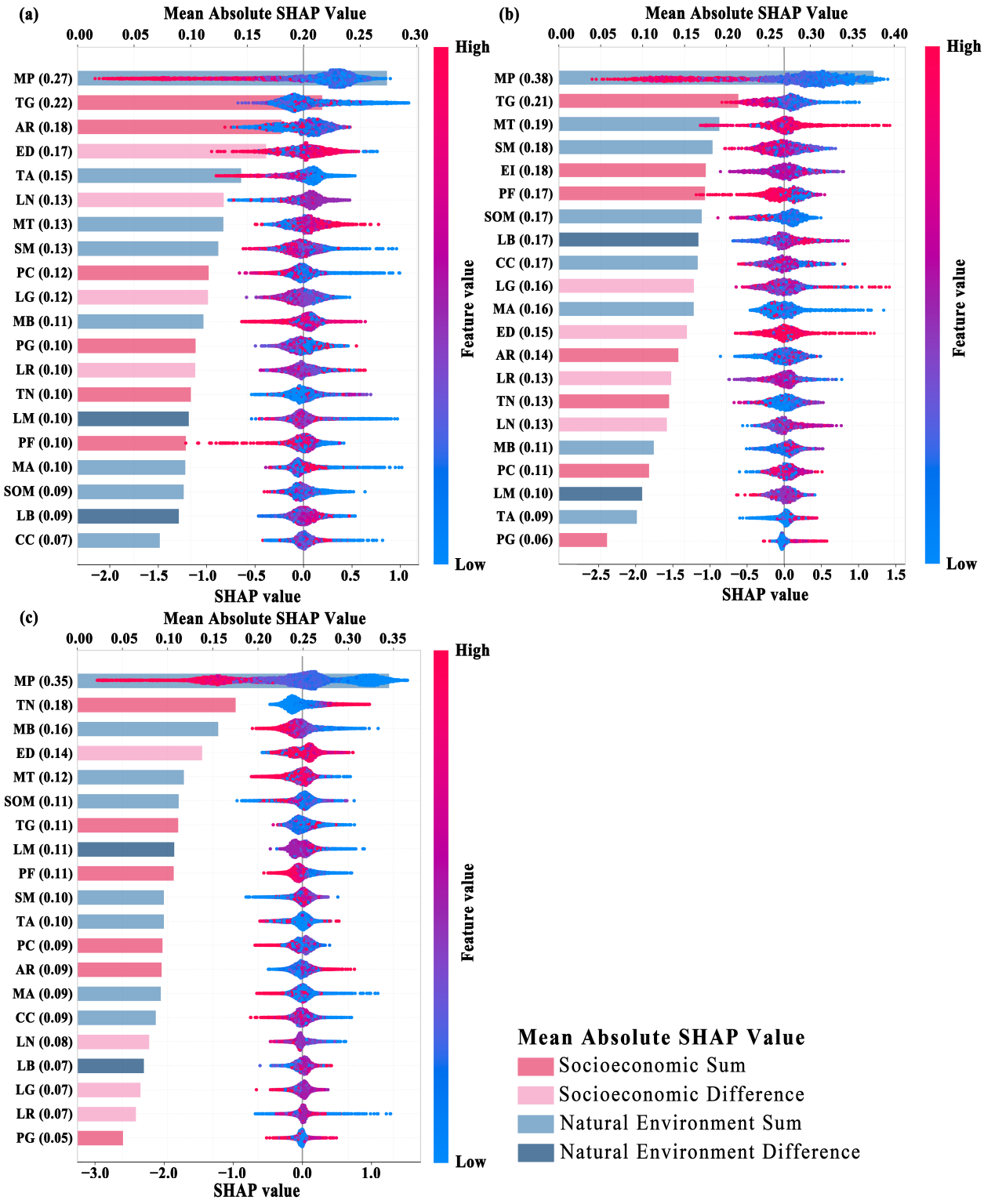


Figure 9. Contribution scores from the XGBoost-SHAP model and corresponding SHAP scatter plots for vegetation resilience gradient types across hierarchical administrative border belts in the BTH region. (**a**) Provincial border belts; (**b**) city border belts; (**c**) county border belts.

The drivers of gradient-effect intensity also exhibit distinct patterns across administrative levels (Figure 10). For provincial border belts, an increase in mean annual precipitation (MP) consistently reduces gradient intensity, while tree age (TA, −0.46) and mean altitude (MA, −0.35) further contribute to this suppression. Conversely, total GDP (TG, 0.40), cross-boundary economic disparity (ED, 0.35), cropland proportion (PF, 0.33), and built-up area

proportion (CC, 0.31) significantly amplify gradient intensity. In county border belts, higher mean temperature (MT, −0.17) serves to weaken gradient intensity, whereas total GDP (TG, 0.25) acts as an intensifying factor. Notably, city border belts display a contrasting pattern: cropland proportion (PF, −0.24) and total GDP (TG, −0.28) reduce gradient intensity, while lateral total GDP difference (LG, 0.26) enhances it, distinguishing city belts from both provincial and county counterparts.

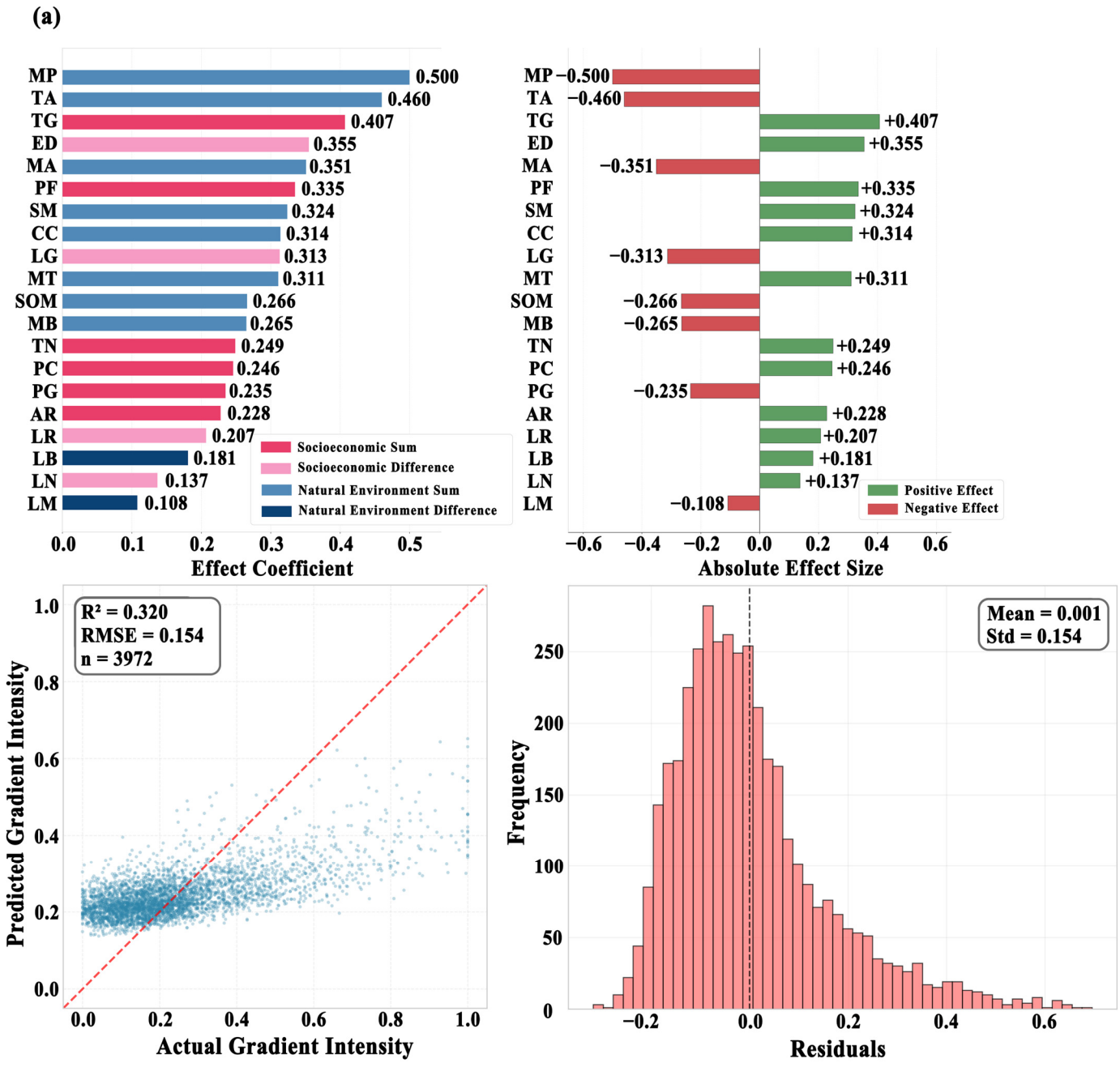


Figure 10. *Cont.*

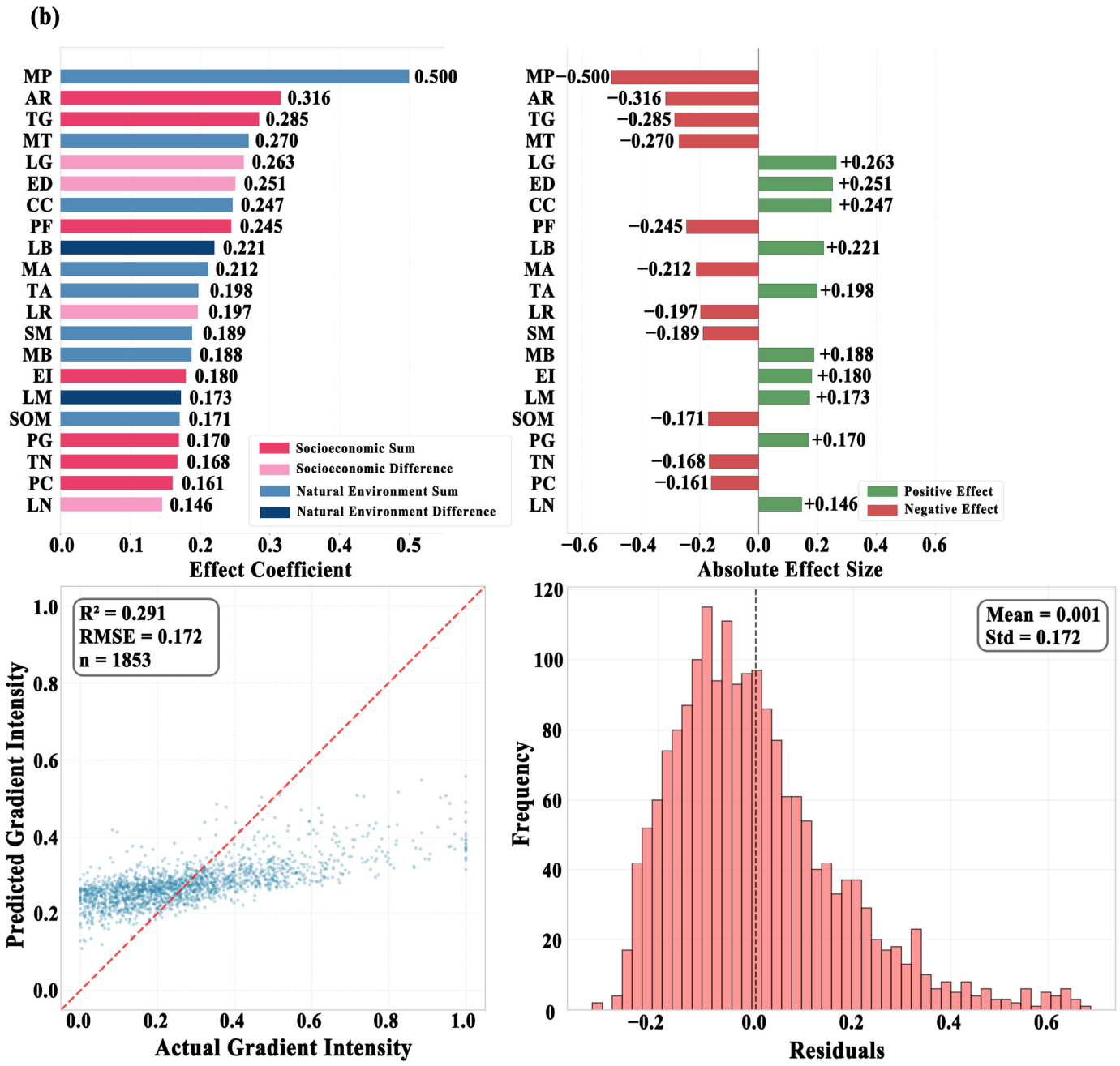


Figure 10. *Cont.*

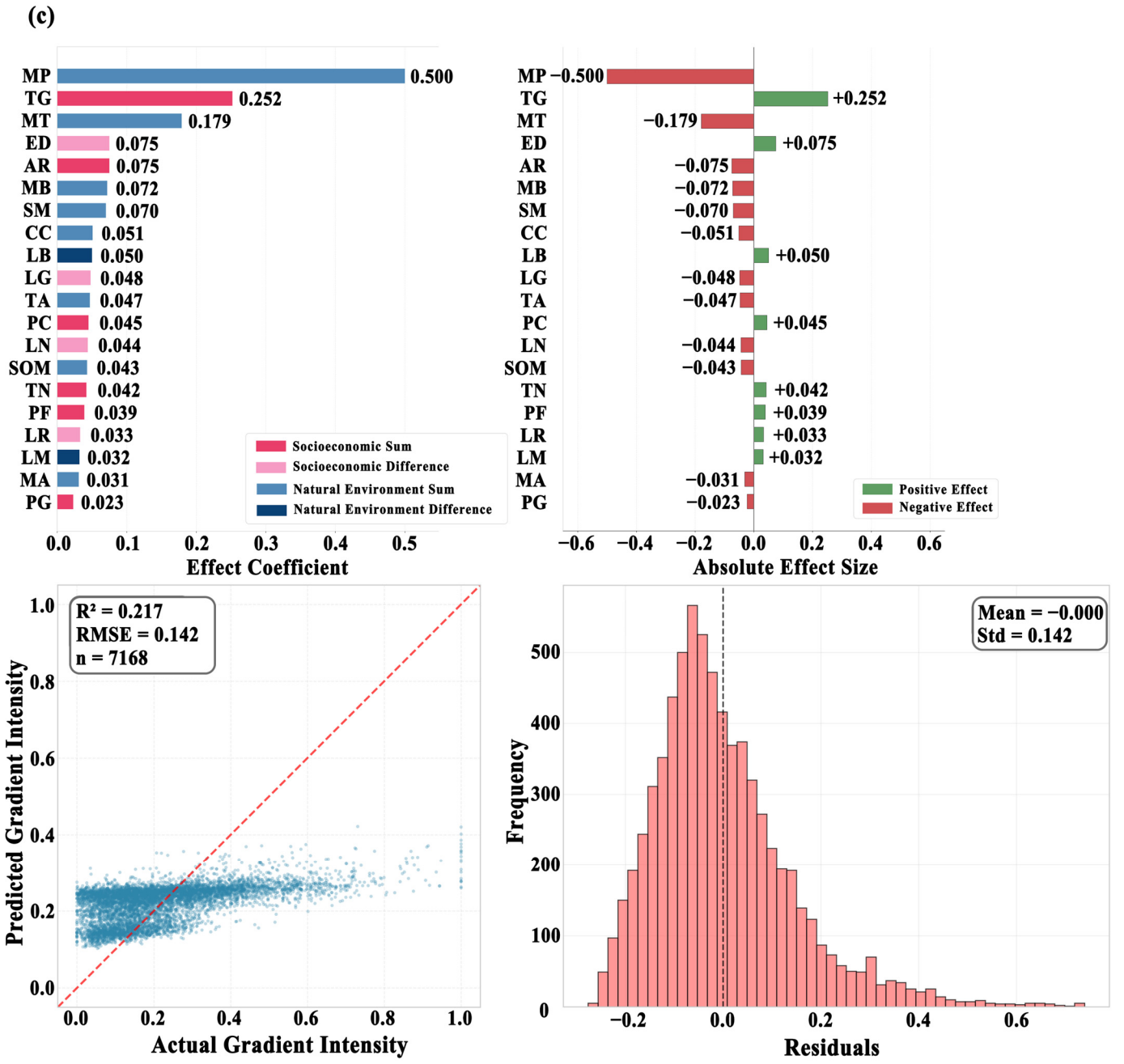


Figure 10. Influencing factors analysis of gradient intensity across three hierarchical administrative border belts in the BTH region. (**a**) Provincial border belts; (**b**) city border belts; (**c**) county border belts.

4. Discussion

4.1. Temporal Decline and Recovery of Vegetation Resilience with a Shift from City to Provincial Optimality in the BTH Region

Most studies have focused on the spatiotemporal dynamics of vegetation resilience at the watershed or regional scale, yet few have specifically investigated the evolutionary characteristics of vegetation resilience within administrative border belts. This lack of research hampers effective cross-jurisdictional ecological coordination. To address this gap, this study assessed vegetation resilience within the provincial, city, and county border belts of the BTH region for the years 2005, 2010, 2015, and 2020, using a long-term NDVI dataset. While 10-year NDVI-based resilience estimates involve overlapping temporal windows

and differing buffer widths across administrative levels, the consistent temporal trends within each level support our main conclusions.

The results reveal that vegetation resilience across the three hierarchical border belts in the BTH region followed a trajectory of initial decline followed by a subsequent recovery. Existing studies have confirmed that the period from 2000 to 2015 witnessed rapid socioeconomic development accompanied by a decline in environmental quality across the BTH region. During this phase, the "growth-first" paradigm likely exerted considerable stress on ecologically fragile zones, particularly administrative border belts [35]. However, since approximately 2010, the implementation of ecological restoration projects has intensified markedly. Notable examples include the Second Phase of the Beijing–Tianjin Sandstorm Source Control Project initiated in 2013 and the cross-jurisdictional ecological compensation mechanism for the watersheds of the Guanting and Miyun Reservoirs [36–38]. These transboundary cooperative restoration efforts have been instrumental in stabilizing vegetation resilience within border belts.

4.2. Pronounced Gradient Effects in Provincial and City Border Belts with a North–South Disparity Across the BTH Region

The analysis of gradient types and intensities revealed a pronounced north–south spatial disparity across the three hierarchical border belts. Northern cities (Zhangjiakou, Tangshan, Langfang, Qinhuangdao) exhibited substantially stronger gradient effects than southern cities (Xingtai, Handan, Hengshui), with Shijiazhuang and Baoding showing moderate effects. This pattern is likely associated with underlying gradients in natural conditions and anthropogenic pressures. The northern BTH region is characterized by greater topographic relief, higher forest cover, and more fragmented landscapes, which may contribute to boundary-induced ecological differences [39,40]. In contrast, the southern plains are dominated by intensive agriculture and more uniform land use, which may reduce the expression of gradient effects. Additionally, cross-boundary disparities in economic development and ecological investment may be more pronounced in the north, potentially further contributing to stronger gradient formation.

Regarding hierarchical differences, gradient effects were most pronounced in provincial and city border belts, while county belts exhibited notably weaker effects. This observation is consistent with the finding that higher administrative levels tend to have larger cross-boundary disparities in policy implementation, fiscal capacity, and land use regulation [41]. Temporally, gradient effects followed a pattern of initial decline followed by recovery from 2005 to 2020, mirroring the broader vegetation resilience trend. By 2020, gradient effects in city and county belts had surpassed 2005 levels, suggesting delayed transmission of ecological restoration benefits from higher to lower administrative tiers. Furthermore, an inverse relationship between vegetation resilience and gradient effects was observed: in 2005, city belts showed higher resilience yet weaker gradient effects, while provincial belts showed lower resilience yet stronger effects; by 2020, this pattern had reversed. This inverse relationship implies that higher resilience tends to diminish gradient effects, whereas lower resilience amplifies them, raising the possibility that targeted ecological restoration in less resilient border zones may effectively mitigate cross-boundary gradient disparities.

4.3. Regulatory Roles of Economic Development and Land-Use Transition in Shaping Gradient Effects

The attribution analysis reveals that natural endowments fundamentally shape vegetation resilience gradient effects across all three administrative levels. Mean annual precipitation (MP) consistently emerges as the most important factor suppressing gradient formation, with contribution scores ranging from 0.27 to 0.37 across provincial, city,

and county borders. This finding aligns with established knowledge that moisture availability governs vegetation growth and recovery capacity, particularly in water-limited ecosystems [42]. When precipitation is abundant, vegetation resilience tends to be more homogeneous across boundaries, dampening potential gradient effects. Similarly, tree age (TA) and mean altitude (MA) further contribute to gradient suppression, suggesting that mature forests and topographically complex terrains buffer against cross-boundary ecological differentiation. These older, well-established ecosystems possess greater stability and resistance to disturbance, reducing the likelihood of abrupt ecological transitions at administrative boundaries [43,44].

Conversely, cross-boundary socioeconomic disparities and land use composition consistently amplify gradient effects across administrative levels. Cross-boundary economic disparity (ED) emerges as a key promoter at both provincial (0.16) and county (0.13) borders, while lateral GDP difference (LG, 0.26) specifically intensifies gradient effects at city borders. This pattern suggests that when adjacent jurisdictions diverge in economic development levels, vegetation resilience tends to differ markedly across the boundary—likely reflecting disparities in fiscal capacity for ecological investment, land use intensity, and environmental regulation stringency [45]. Land use factors further modulate gradient effects in a hierarchical manner. In provincial border belts, higher cropland proportion (PF, 0.33) and built-up area proportion (CC, 0.31) significantly amplify gradient intensity, indicating that agricultural expansion and urbanization create sharper ecological contrasts across boundaries. In contrast, city border belts display a reversed pattern, where cropland proportion (PF, −0.24) reduces gradient intensity. This contrast is consistent with the hypothesis that inter-jurisdictional coordination differs systematically across administrative levels. At the city level, borders fall within the same provincial administrative framework, where unified policies, planning mandates, and fiscal arrangements promote more coherent land use and ecological restoration coordination across city boundaries [46]. At the provincial level, however, borders separate independent administrative entities with their own development priorities, environmental standards, and fiscal capacities, making coordinated cross-boundary land management inherently more difficult [47,48]. This institutional asymmetry—where coordination is structured within provinces but largely absent between them—offers a plausible explanation for why land use intensification amplifies gradient effects at provincial borders but not at city borders. That said, landscape composition differences or scale-dependent confounding may also contribute to the observed pattern, and direct examination of cross-jurisdictional policy variables or coordination indices would be valuable to further validate this interpretation. The amplifying effect of nighttime light differences (LN, 0.13; TN, 0.17) further supports this interpretation, as nighttime illumination serves as a reliable proxy for urbanization intensity and economic activity [49]. These findings suggest that enhancing inter-provincial coordination mechanisms for land use planning and ecological restoration—similar to the more integrated intra-provincial model—could significantly mitigate cross-boundary gradient effects, highlighting the need for strengthened regional governance frameworks alongside targeted conservation interventions.

4.4. Cross-Border Governance Strategies Based on Gradient Effect Analysis

The observed shift in resilience optimality from city to provincial borders by 2020 underscores the critical role of higher administrative levels in driving vegetation recovery, while also revealing that city and county border belts continue to lag behind in resilience gains. Although provinces have benefited from concentrated ecological restoration funding and unified planning mandates, lower administrative tiers have experienced slower recovery, as reflected in the persistently lower resilience gains at city and county levels compared

to provincial belts [50]. This disparity points to the need for effective ecological restoration that requires not merely project implementation but also strengthened cross-jurisdictional coordination, increased financial support for local-level initiatives, and the integration of lower-tier border belts into broader provincial planning frameworks [51]. Specifically, the observed delayed recovery at county borders suggests that extending provincial-level restoration funding mechanisms to municipal and county border zones could accelerate resilience gains at lower administrative tiers.

The pronounced north–south disparity in gradient effects—with northern belts (Zhangjiakou, Tangshan, Langfang, Qinhuangdao) exhibiting substantially stronger effects than their southern counterparts—highlights priority areas for intervention. Given the strong gradient effects in Zhangjiakou and Tangshan, where gradient effect types reached 45.80% and 43.53%, respectively, priority interventions should focus on these two cities. Specific actions could include harmonizing land use policies between adjacent provinces (e.g., Hebei and Inner Mongolia for Zhangjiakou) and aligning conservation investments across provincial borders. Joint monitoring programs targeting vegetation resilience and gradient indicators (e.g., NDVI trends, proportion of gradient effect types) should be established in these high-gradient zones to track intervention effectiveness. Conversely, southern belts, where gradient effects are weaker, may benefit from less intensive interventions focused on maintaining existing land use continuity and preventing future divergence.

The influence mechanisms reveal several actionable insights for cross-border governance. Natural factors—particularly precipitation, tree age, and altitude—show consistent associations with gradient effects, and that ecologically sensitive zones (e.g., mature forests, high-altitude areas) should be prioritized as natural buffers. The contrasting roles of land use across administrative levels suggest a differentiated governance pathway. At provincial borders, the finding that cropland proportion (PF, 0.33) and built-up area (CC, 0.31) are associated with amplified gradient intensity suggests that inter-provincial coordination in land use planning and ecological restoration should prioritize agricultural and urban expansion control—particularly in high-gradient areas such as the Zhangjiakou border zone. Quantitatively, reducing cropland expansion by 10% in these zones could potentially reduce gradient intensity by approximately 0.03 based on our coefficient estimates. At city borders, where cropland proportion is unexpectedly associated with reduced gradient intensity, existing intra-provincial coordination appears more effective, potentially providing a foundation for higher-level cooperation. The finding that cross-boundary economic disparity (ED, 0.16 at provincial borders) and nighttime light differences (LN, 0.13; TN, 0.17) amplify gradient effects further indicates that convergence in economic development and urbanization intensity across borders—particularly reducing the GDP and nighttime light gaps between adjacent provinces—could complement ecological restoration in mitigating gradient effects. This suggests that joint land use zoning, cross-boundary ecological compensation mechanisms tied to economic performance indicators, and harmonized environmental standards between neighboring provinces are priority policy instruments. The amplifying effects of economic disparity and nighttime light differences further indicate that socioeconomic convergence, alongside ecological restoration, is essential for reducing cross-boundary ecological contrasts. Integrated governance strategies should thus combine targeted interventions in high-gradient zones with policies that promote economic and infrastructural alignment across administrative boundaries.

4.5. Limitations

While this study reveals the spatiotemporal patterns and driving mechanisms of vegetation resilience gradient effects across hierarchical border belts in the BTH region, several limitations warrant consideration. First, vegetation resilience was estimated using

annual NDVI data based on the AR(1) model; future research could employ monthly or higher-frequency remote sensing data (e.g., MODIS, Sentinel-2) to test the robustness of the findings and capture finer-scale resilience dynamics. Second, this study systematically examined gradient effect types and intensities, yet the spatial range thresholds of gradient effects—identified via Pettitt change-point detection—merit further validation through alternative statistical methods or field-based investigations. Third, the selected buffer widths (15 km, 10 km, and 5 km) correspond to administrative hierarchies, though alternative distance thresholds could be tested to assess result robustness. Future research integrating higher-resolution remote sensing, field observations, and comparative methodological approaches would provide deeper insight into the coupled natural-governance systems shaping vegetation dynamics across administrative borders.

5. Conclusions

Administrative border belts represent critical yet often neglected zones where fragmented governance can hinder ecological recovery. Understanding the gradient effects of vegetation resilience across hierarchical administrative boundaries is therefore essential for effective cross-jurisdictional coordination. This study systematically assessed vegetation resilience and its gradient effects across provincial, city, and county border belts in the BTH from 2005 to 2020. By integrating GAMs, random forest and XGBoost-SHAP analysis, the spatiotemporal patterns, gradient types, intensity dynamics, and underlying mechanisms were elucidated. The main findings are as follows:

(1) Vegetation resilience across the three hierarchical border belts followed a trajectory of initial decline followed by recovery, with a marked shift in resilience optimality from city belts in 2005 to provincial belts by 2020. Gradient effects exhibited pronounced north–south spatial disparity, with northern cities showing substantially stronger effects than southern counterparts, which may be partly associated with greater topographic relief and differences in ecological restoration investments in the north, potentially contributing to cross-city and cross-county disparities. Among the five gradient types, the stable-fluctuating type was consistently predominant across all levels, followed by peak and valley types.

(2) Natural endowments appear to play a fundamental role in shaping gradient effects, with mean annual precipitation, tree age, and altitude consistently associated with the suppression of gradient formation. Conversely, cross-boundary economic disparity, nighttime light differences, and land use composition—particularly cropland and built-up expansion—amplify gradient effects. Notably, these factors modulate effects hierarchically—agricultural and urban expansion intensify gradients at provincial borders but reduce them at city borders, suggesting a potential role of governance coordination.

(3) Based on these findings, a tiered governance framework is proposed: northern high-gradient provincial and city borders—particularly Zhangjiakou and Tangshan—should receive the highest priority for intensive interventions, given their pronounced gradient effects and critical roles as ecological barriers. Targeted actions in these zones should include harmonizing land use policies across provincial boundaries, aligning conservation investments, and establishing joint monitoring programs tracking NDVI trends and gradient dynamics. For county borders, where gradient effects are weakest and model explanatory power is lowest, we recommend moderate, low-intensity interventions focused on maintaining land use continuity and preventing future divergence, rather than large-scale restoration prioritization. At the provincial level, stronger inter-provincial coordination via cross-boundary ecological compensation and harmonized environmental standards should be pursued to mitigate gradient effects. Additional financial and technical support should be directed toward lagging county-level areas within broader provincial planning

frameworks to prevent further divergence, though with appropriate caution given the lower predictive certainty at this scale.

Collectively, this study advances the scientific understanding of vegetation resilience gradient effects across administrative hierarchies and offers a framework for cross-jurisdictional ecological governance in the BTH region and other analogous urban agglomerations.

Supplementary Materials: The following supporting information can be downloaded at: https://www.mdpi.com/article/10.3390/land15071321/s1, Figure S1: Effective range of gradient effects for border belts; Figure S2: Representative examples of gradient effect identification across provincial, city, and county border belts; Figure S3: XGBoost-SHAP model performance for provincial, city and county border belts.

Author Contributions: Conceptualization, L.Z. and Y.Z.; methodology, K.W.; software, R.L.; validation, R.L., Y.Z. and K.W.; formal analysis, L.Z.; investigation, Y.Z.; resources, S.W.; data curation, T.Q. and L.L.; writing—original draft preparation, L.Z.; writing—review and editing, Y.Z.; visualization, R.L.; supervision, Y.Z.; project administration, Y.Z.; funding acquisition, Y.Z. All authors have read and agreed to the published version of the manuscript.

Funding: This research was funded by the "National Key Research and Development Plan Program" (No. 2024YFD2200900).

Data Availability Statement: Data will be made available on request.

Conflicts of Interest: The authors declare no conflicts of interest.

References

1. Piao, S.L.; Wang, X.H.; Park, T.; Chen, C.; Lian, X.; He, Y.; Bjerke, J.W.; Chen, A.P.; Ciais, P.; Tommervik, H.; et al. Characteristics, drivers and feedbacks of global greening. *Nat. Rev. Earth Environ.* **2020**, *1*, 14–27. [CrossRef]
2. Zhong, J.; Liu, J.; Jiao, L.; Geiß, C.; Droin, A.; Taubenböck, H. Unveiling the spatio-temporal patterns of vegetation growth influenced by diverse urban intensity gradients. *Environ. Impact Assess. Rev.* **2025**, *112*, 107810. [CrossRef]
3. Wang, B.; Wen, Z.; Que, P.; Zhang, T.; He, X.; Yang, N.; Zhong, X.; Xu, Y. Biodiversity benefits of China's 20-year efforts in forest restoration. *Nat. Commun.* **2025**, *16*, 10724. [CrossRef] [PubMed]
4. Xiao, C.; Wang, Y.; Feng, Z.; Huan, S.; Yue, Z.; Peñuelas, J.; Zhang, M.; Dong, H.; Wu, C. Global cropland loss at borders contributes to increased biodiversity. *Commun. Earth Environ.* **2025**, *6*, 957. [CrossRef]
5. Jiang, X. No County is an Island: The Rise of Interjurisdictional Cooperation among Counties in China. *Reg. Stud.* **2022**, *56*, 1719–1734. [CrossRef]
6. Kark, S.; Levin, N.; Grantham, H.S.; Possingham, H.P. Between-country collaboration and consideration of costs increase conservation planning efficiency in the Mediterranean Basin. *Proc. Natl. Acad. Sci. USA* **2009**, *106*, 15368–15373. [CrossRef] [PubMed]
7. Qiao, J.; Deng, L.; Liu, H.; Wang, Z. Spatiotemporal heterogeneity in ecosystem service trade-offs and its driving factors in the Huang-Huai-Hai Plain. *Landsc. Ecol.* **2024**, *39*, 42. [CrossRef]
8. Yue, Z.; Xiao, C.; Feng, Z.; Wang, Y.; Yan, H. Accelerating decline of habitat quality in Chinese border areas. *Resour. Conserv. Recycl.* **2024**, *206*, 107665. [CrossRef]
9. Xue, S.; Xiao, H.; Ren, J. Cross-border interactions on the sustainable development between global countries. *Resour. Conserv. Recycl.* **2024**, *204*, 107525. [CrossRef]
10. Wang, P.; Lu, R.; Fan, T.; Zhang, L.; Nong, X. Integrated optimization of border ecosystem services and risks: A multiscale exploration considering the past and future. *Environ. Impact Assess. Rev.* **2025**, *115*, 107986. [CrossRef]
11. Yao, Y.; Liu, Y.; Fu, F.; Song, J.; Wang, Y.; Han, Y.; Wu, T.; Fu, B. Declined terrestrial ecosystem resilience. *Glob. Change Biol.* **2024**, *30*, e17291. [CrossRef] [PubMed]
12. Kong, Z.; Ling, H.; Deng, M.; Long, A.; Zhang, Y.; Zhang, Y.L. Decoupled greening and vegetation resilience in the arid Tarim River mainstream and its driving mechanisms. *J. Clean. Prod.* **2026**, *554*, 148123. [CrossRef]
13. Wu, N.; Zhou, Y.; Yin, S.; Gong, H.; Zhang, C. Revealing the nonlinear impact of environmental regulation on ecological resilience using the XGBoost-SHAP model: Evidence from the Yangtze River Delta region, China. *J. Clean. Prod.* **2025**, *514*, 145700. [CrossRef]
14. Liu, J.; Dietz, T.; Carpenter, S.R.; Alberti, M.; Folke, C.; Moran, E.; Pell, A.N.; Deadman, P.; Kratz, T.; Lubchenco, J.; et al. Complexity of coupled human and natural systems. *Science* **2007**, *317*, 1513–1516. [CrossRef] [PubMed]

15. Lambin, E.F.; Meyfroidt, P. Global land use change, economic globalization, and the looming land scarcity. *Proc. Natl. Acad. Sci. USA* **2011**, *108*, 3465–3472. [CrossRef] [PubMed]
16. Cui, L.; Shen, Z.; Liu, Y.; Yu, C.; Lu, Q.; Zhang, Z.; Gao, Y.; Nie, T. Identification of driving forces for windbreak and sand fixation services in semiarid and arid areas: A case of Inner Mongolia, China. *Prog. Phys. Geog.* **2023**, *47*, 32–49. [CrossRef]
17. Scherer-Lorenzen, M.; Gessner, M.O.; Beisner, B.E.; Messier, C.; Paquette, A.; Petermann, J.S.; Soininen, J.; Nock, C.A. Pathways for cross-boundary effects of biodiversity on ecosystem functioning. *Trends Ecol. Evol.* **2022**, *37*, 454–467. [CrossRef] [PubMed]
18. Adame, M.F.; Hermoso, V.; Perhans, K.; Lovelock, C.E.; Herrera-Silveira, J.A. Selecting cost-effective areas for restoration of ecosystem services. *Conserv. Biol.* **2014**, *29*, 493–502. [CrossRef] [PubMed]
19. Didan, K. *MODIS/Terra Vegetation Indices 16-Day L3 Global 500m SIN Grid V061 [DS]*; NASA Land Processes Distributed Active Archive Center: Sioux Falls, SD, USA, 2021. [CrossRef]
20. Xu, X. *1 km Grid GDP Distribution Data of China (2015)*; Resource and Environmental Science Data Registration and Publishing System: Beijing, China, 2019. [CrossRef]
21. Li, Y.; Dai, L. *China "DMSP-OLS-like" 1 km Nighttime Light Remote Sensing Dataset (1992–2024)*; National Earth System Science Data Center: Beijing, China, 2025. [CrossRef]
22. Zhang, Z.; Chase, J.M.; Bearup, D.; Liao, J. Complex interactive responses of biodiversity to multiple environmental drivers. *Ecology* **2024**, *106*, e4484. [CrossRef] [PubMed]
23. Peng, S. *Monthly Precipitation Dataset for China at 1-km Resolution (1901–2024)*; National Earth System Science Data Center: Beijing, China, 2025. [CrossRef]
24. Peng, S. 1 km monthly temperature and precipitation dataset for China from 1901 to 2017. *Earth Syst. Sci. Data* **2019**, *11*, 1931–1946. [CrossRef]
25. Shang, R.; Lin, X.; Chen, J.M.; Liang, Y.; Fang, K.; Xu, M.; Yan, Y.; Ju, W.; Yu, G.; He, N.; et al. China's annual forest age dataset at a 30 m spatial resolution from 1986 to 2022. *Earth Syst. Sci. Data* **2025**, *17*, 3219–3241. [CrossRef]
26. Nguyen, C.T.; Vačkářová, D.; Weinzettel, J. Consistent global dataset on biodiversity intactness footprint of agricultural production from 2000 to 2020. *Sci. Data* **2025**, *12*, 1613. [CrossRef] [PubMed]
27. Geospatial Data Cloud. Global 30m DEM Dataset [DS]. Available online: https://www.gscloud.cn/sources/details/aeab8000652a45b38afbb7ff023ddabb?pid=302 (accessed on 12 November 2025).
28. Dai, Y.; Shangguan, W. *Dataset of Soil Properties for Land Surface Modeling Over China*; A Big Earth Data Platform for Three Poles: Beijing, China, 2019. [CrossRef]
29. Ingrisch, J.; Bahn, M. Towards a comparable quantification of resilience. *Trends Ecol. Evol.* **2018**, *33*, 251–259. [CrossRef] [PubMed]
30. Wood, S.N. *Generalized Additive Models: An Introduction with R*, 2nd ed.; Chapman and Hall/CRC: Boca Raton, FL, USA, 2017. [CrossRef]
31. Lai, J.; Tang, J.; Li, T.; Zhang, A.; Mao, L. Evaluating the relative importance of predictors in Generalized Additive Models using the gam.hp R package. *Plant Divers* **2024**, *46*, 542–546. [CrossRef] [PubMed]
32. Huang, X.; Liu, X.; Jin, Y.; Gao, X.; Chen, Y. Identification and attribution analysis of integrated ecological zones based on the XGBoost-SHAP model: A case study of Chengdu, China. *Ecol. Indic.* **2025**, *177*, 113787. [CrossRef]
33. Simon, S.M.; Glaum, P.; Valdovinos, F.S. Interpreting random forest analysis of ecological models to move from prediction to explanation. *Sci. Rep.* **2023**, *13*, 3881. [CrossRef] [PubMed]
34. Zhang, L.; Huettmann, F.; Liu, S.; Sun, P.; Yu, Z.; Zhang, X.; Mi, C. Classification and regression with random forests as a standard method for presence-only data SDMs: A future conservation example using China tree species. *Ecol. Inform.* **2019**, *52*, 46–56. [CrossRef]
35. Wei, Y.Y.; Wang, D.Y.; Yang, Y.Y.; Zou, L.L.; Wu, S.Z. Evaluating the sustainability of rural territorial system with a social-ecological system framework: A case of Beijing-Tianjin-Hebei region, China. *Habitat Int.* **2026**, *169*, 103727. [CrossRef]
36. Yang, Q.; Liu, G.Y.; Agostinho, F.; Giannetti, B.F.; Yang, Z.F. Assessment of ecological restoration projects under water limits: Finding a balance between nature and human needs. *J. Environ. Manag.* **2022**, *311*, 114849. [CrossRef] [PubMed]
37. Hou, W.; Zhai, L.; Walz, U. Identification of spatial conservation and restoration priorities for ecological networks planning in a highly urbanized region: A case study in Beijing-Tianjin-Hebei, China. *Ecol. Eng.* **2023**, *187*, 106859. [CrossRef]
38. Zheng, L.F.; Rong, Y.J.; Wang, K.P.; Liu, C.H.; Zhang, Y.L.; Yan, Y. When Will Green Miracle Work? Spatiotemporal Pattern Analysis of Ecological Restoration's Effect in Arid, Semiarid Regions. *Ecosyst. Health Sustain.* **2026**, *12*, 0500. [CrossRef]
39. Antonelli, A.; Kissling, W.D.; Flantua, S.G.A.; Bermúdez, M.A.; Mulch, A.; Muellner-Riehl, A.N.; Kreft, H.; Linder, H.P.; Badgley, C.; Fjeldså, J.; et al. Geological and climatic influences on mountain biodiversity. *Nat. Geosci.* **2018**, *11*, 718–725. [CrossRef]
40. Gao, J.; Wang, Y.; Zou, C.; Xu, D.; Lin, N.; Wang, L.; Zhang, K. China's ecological conservation redline: A solution for future nature conservation. *Ambio* **2020**, *49*, 1519–1529. [CrossRef] [PubMed]
41. Zhang, T.; Gibson, L.; Ma, J.; Sreekar, R.; Lindenmayer, D.; Liu, J. Global patterns of border protected areas reveal gaps in transboundary conservation efforts. *One Earth* **2025**, *8*, 101206. [CrossRef]

42. Stein, A.; Gerstner, K.; Kreft, H. Environmental heterogeneity as a universal driver of species richness across taxa, biomes and spatial scales. *Ecol. Lett.* **2014**, *17*, 866–880. [CrossRef] [PubMed]
43. Toriyama, J.; Hashimoto, S.; Nakao, K.; Saitoh, T.M.; Nishizono, T.; Uchiyama, K.; Araki, M.G.; Murakami, W.; Hirata, Y. Management strategies for shrinking and aging tree plantations are constrained by the synergies and trade-offs between carbon sequestration and other forest ecosystem services. *J. Environ. Manag.* **2025**, *373*, 123762. [CrossRef] [PubMed]
44. Barbosa, A.; Barbosa, B.; Sousa, T.S.; Fares, A.L.B.L.; Barbosa, E.D.E.S.; Ribeiro, S.C.; Schmidt, F.A.; Teodoro, G.S. Age-driven shifts in functional composition and diversity shape ecosystem service provision in agroforestry systems. *Sci. Total Environ.* **2026**, *1017*, 181497. [CrossRef] [PubMed]
45. Liu, J.; Zhang, Q.; Hu, Y. Regional differences of China's urban expansion from late 20th to early 21st century based on remote sensing information. *Chin. Geogr. Sci.* **2012**, *22*, 1–14. [CrossRef]
46. Liu, Y.; Liu, R.; Chen, J.M. Retrospective retrieval of long-term consistent global leaf area index (1981–2011) from combined AVHRR and MODIS data. *J. Geophys. Res. Biogeosciences* **2015**, *117*, G04003. [CrossRef]
47. Gu, G.; Wu, B.; Lu, S.; Zhang, W.; Tian, Y.; Lu, R.; Feng, X.; Liao, W. Differential evolution of territorial space and effects on ecological environment quality in China's border regions. *J. Geogr. Sci.* **2024**, *34*, 1109–1127. [CrossRef]
48. Zhang, D.; Yuan, W.; Liu, P.; Ju, Z. Vertical and horizontal ecological compensation of the Taihu Lake Basin based on ecosystem services value. *Environ. Dev. Sustain.* **2025**. [CrossRef]
49. He, X.; Xu, K.; Jiang, S.; Zhao, P.; Zuo, X.; Wang, S. Urbanization intensity and its effect on vegetation phenology in urban areas and beyond: Evidence from three representative cities in the Yangtze river delta. *Urban Ecosyst.* **2026**, *29*, 40. [CrossRef]
50. Zhang, Y.Z.; Wang, J.; Zhang, M.; He, C.F. The mechanism of revoking counties or county-level cities to municipal districts and its effect on urban expansion in Chinese cities. *Environ. Dev. Sustain.* **2023**, *159*, 103068. [CrossRef]
51. Decoville, A.; Durand, F. An empirical approach to cross-border spatial planning initiatives in Europe. *Reg. Stud.* **2021**, *55*, 1417–1428. [CrossRef]

Disclaimer/Publisher's Note: The statements, opinions and data contained in all publications are solely those of the individual author(s) and contributor(s) and not of MDPI and/or the editor(s). MDPI and/or the editor(s) disclaim responsibility for any injury to people or property resulting from any ideas, methods, instructions or products referred to in the content.